Chapter 5

Conducting Polymers Incorporated with Related Graphene Compound Films for Use for Humidity and NH_3 Gas Sensing

Nguyen Nang Dinh

Additional information is available at the end of the chapter

http://dx.doi.org/10.5772/intechopen.79060

Abstract

Using spin-coating technique, PEDOT:PSS+GQD+CNT (GPC), PEDOT:PSS+GQD+AgNW (GPA) films used for humidity sensors and P3HT + rGO + CNT (P3GC) films used for NH_3 gas sensors were prepared. At room temperature and atmospheric pressure, all the sensing devices have extremely simple structure and they respond well to the humidity change (for GPC and GPA) and NH_3 gas (for P3GC). The sensitivity of both the GPC and GPA humidity sensing devices was found to be dependent on the additives of CNT or AgNW. For the GPA sensors, the best sensitivity attained a value as large as 15.2% with a response time of 30 s. For the NH_3 gas sensors made from P3GC films with a content of 20 wt.% of rGO and 10% of CNTs, the best performance parameters were obtained, such as responding time of ca. 30 s, sensing response of 0.8% at ammonia gas concentration of 10 ppm and a relative sensitivity of 0.05%/ppm. The fact that the P3HT + rGO + CNT sensors do not respond to humidity suggests useful applications in gas thin-film sensors for selectively sensing ammonia gas in a humid environment.

Keywords: graphene quantum dots (GQDs), polymeric nanocomposite, surface morphology, humidity and NH_3 sensing, sensing response and sensitivity

1. Introduction

Nanocomposites are known as materials mixing two or more different materials, where at least one of these having a nanodimensional phase, for example, conjugate polymers embedded with metallic, semiconducting, and dielectric nanoparticles. In comparison with devices made from standard materials, the nanocomposites based devices usually possess enhanced

efficiency and service life [1–4]. This is because inorganic nanoparticles embedded in conducting polymers can improve the mechanical, electrical, and optical properties such as nonlinear optical behavior, photoluminescence, electroluminescence, and photoconductivity [5–7]. Nanostructured composites or nanohybrid layers containing numerous heterojunctions can be utilized for optoelectronics, organic light emitting diodes (OLEDs), organic solar flexible cells (OSC) [8, 9], etc. Among conducting polymers, polyethylenedioxythiophene:poly(4-styrenesulfonate) (abbreviated to PEDOT:PSS) as a p-type organic semiconductor is well used for the hole transport layer in OLED [10] and OSC [4] as well as for the matrix materials in various sensors [11]. Various nanocomposite films consisting of conducting polymers mixed with carbon nanotubes (CNT) as an active material have been prepared for application in gas thin-film sensors. Recently, Olenych et al. [12] used hybrid composites based on PEDOT:PSS-porous silicon-CNT for preparation and characterization of humidity sensors. The value of the resistance of the hybrid films was as large as 10 MΩ that may have caused a reduced accuracy in monitoring the resistance change versus humidity.

It is known that graphene possesses many excellent electrical properties, since it is an allotrope of carbon with a structure of a single two-dimensional (2D) layer of sp^2 hybridized carbon atoms. Graphene quantum dots (GQDs), as seen in [13, 14], are a kind of 0D material made from small pieces of graphene. GQDs exhibit new phenomena due to quantum confinement and edge effects, which are similar to semiconducting QDs [15]. Graphene and related materials like graphene oxide (GO) or reduced graphene oxide (rGO) as materials used for chemical sensing have significant application potential. This is due to the two-dimensional structure that results in a high sensing area per unit volume and a low noise compared to other solid-state sensors. There were many works reporting on the use of graphene or graphene-related materials for monitoring gases and vapors [16, 17]. Especially, some of the works attempted to connect the advantages of nanoscale metals with that of graphene for the improvement of gas sensor applications [18, 19]. GQDs were mainly used in a single-electron transistor (SET). Besides detecting charge in SETs, GQDs have also been recruited to build electronic sensors for the detection of humidity and pressure [20].

Ammonia is a compound of nitrogen and hydrogen with the formula NH_3; it contributes significantly to the nutritional needs of terrestrial organisms by serving as a precursor to food and fertilizer. With the development of the chemical industry, more and more generation of ammonia gas is brought into the environment. It is known that ammonia gas is a toxic compound; consequently, it is harmful to human health when a large enough concentration of this compound is attained [21]. Thus, production of devices (or sensors) to detect ammonia gas with a large sensitivity and selective property is very important. Many scientific groups have researched and developed gas ammonia sensors for applications. Sensors based on nanostructured inorganic structures like SnO_2, WO_3, TiO_2, etc., have large sensitivity and response time, but the technology for producing both the materials and devices for gas sensors usually requests vacuum and high temperature that results in considerably large expenses [22]. With the aim to reduce these costs, many scientific groups have developed gas sensors based on conducting polymers [23–25]. The advantage of the polymer-based sensors consists of easy fabrication, low power consumption, room temperature operation, etc. [26]. Among the conducting polymers, polyethylenedioxythiophene + poly(4-styrenesulfonate)

(PEDOT:PSS) is the most utilized in organic light-emitting diode (OLED) and in organic solar cells (OSCs). PEDOT:PSS is also used for producing gas like CO [27], NH_3 [17], and vapors of organic solvents or water [18, 19]. We recently reported that PEDOT:PSS-based sensors can detect both ammonia gas [28] and humidity [29]. We have in particular observed that PEDOT:PSS + rGO + AgNWs-based sensors are sensitive to relative humidity (RH%) at a value as low as 30% [29]. This ability for detecting humidity is however a disadvantage when monitoring ammonia or other gases in a humid environment is considered. For practical applications, we need a sensor that is not only sensitive to the gas to be measured, but also selectively detecting toward the gas. During our study of OSCs using poly(3-hexylthiophene) (P3HT) as a photoactive layer [4], we recognized that P3HT films synthetized in air with a humidity larger than RH%60 exhibited a quality as good as when it was synthetized in a dried nitrogen glove-box. This would show that the P3HT structure was not affected by the absorption of water vapor. This observation prompted us to investigate the preparation and characterization of potential P3HT-based sensors for selectively detecting ammonia gas, even in a humid environment.

In this work, we report results of our investigation on the fabrication of graphene-quantum dots and nanocomposites of PEDOT:PSS + GQDs+CNT and P3HT + rGO + CNT. The humidity- and NH_3-sensing properties, respectively, of the first and the second composite films are also presented. Comparison of gas-sensing properties between P3HT- and PEDOT:PSS-based composite films is also made.

2. Experimental

2.1. Samples preparation

2.1.1. Preparation of PEDOT-PSS + GQD + CNT (GPC) and PEDOT-PSS + GQD + AgNW (GPA) humidity sensors

Firstly, GQDs were prepared; for this, a solution of graphite flake (GF), $KMnO_4$, and HNO_3 with a weight ratio of 0.2 g:0.2 g:0.4 ml was prepared and put in a Pt crucible. This solution was then put in a microwave heaven for heating in 1 min to separate GF into laminar form (EG). The second solution was made from 0.2 g $NaNO_3$ + 9.6 ml H_2SO_4 (98%) + 1.2 g $KMnO_4$ (called as NKH). EG was mixed with NKH solution and carefully stirred by use of a magnetic device for 2 h to have a GO solution. Adding to the GO solution 30 ml distilled water, and then 10 ml H_2O_2 allowed us to get a dark-yellow solution. By spinning with a rate of 7000 rpm for 5 min, a GO powder was obtained and it was diluted in deionized water. In the next step, NH_3 was added in the solution and stirred at 100°C for 5 h until a solution with a uniform dispersion of GQDs was reached. Finally, the GQDs dispersed solution was filtrated by using the "Dialysis" funnel to collect GQD powder with a volume of 0.2 g. This powder then was dissolved in 20 ml of twice-distilled water to get GQD-dispersion solution of 10 wt.% GQDs (abbreviated to GQD10).

Next, GQD + PEDOT:PSS + CNT composite solutions were prepared. Firstly, a powder of multiple wall carbonate tubes (shortly abbreviated to CNT) with an average size of 30 nm in diameter

and 2 μm in length was embedded in 10 ml of the GQD10 solution without CNT and with three contents of CNT, respectively, 0.5, 1.0, and 1.5 mg. All of the solutions obtained are called GQC solutions. These solutions were treated by plasma in a microwave oven. Then, 2 ml of polyethylene-dioxythiophene + PEDOT:PSS (1.25 wt.% in H_2O) was poured into each GQC solution. The solutions of GQDs-PEDOT:PSS without and with CNT of the three abovementioned volumes of CNT were stirred by ultrasonic wave for 1 h. From all the volumes of chemicals such as GQDs, PEDOT:PSS, and CNT used for the film preparation, the CNT weight contents (wt.%) in the GQDs-PEDOT:PSS matrix have been calculated. It is seen that the samples embedded with the CNT volume of 0.5, 1.0, and 1.5 mg consist of 0.4, 0.8, and 1.2 wt.%, respectively.

Synthesis of Ag nanowires (AgNW) was carried out as follows. Firstly, 20 ml of ethylene glycol was heated within stirring in a 250ml Corning-0215 glass at 70°C for 15 min; then, 17 mg of NaCl was added. Raising temperature up to 100°C, 20 mg of $AgNO_3$ was filled into the glass. The reaction between NaCl and $AgNO_3$ occurred, resulting in formation of opaque AgCl solution. Ethylene glycol was decomposed in aldehyde that played a role of a catalyst for creating Ag nuclei. The next step, 5 mg of KBr was added to the glass and heated up to 140°C for 10 min, following 300 mg of PVP was filled and raising temperature to 160°C. The solution temperature was maintained for 15 min. Finally, 250mg of $AgNO_3$ was added into the solution. The last solution was kept at 160°C for 30 min for growing silver nanowires. In the duration of this time, one can observe the change of the solution color from opaque to bright-gray, proving the formation of AgNWs in the solution. After the solution was cooled automatically to room temperature (in ~90 min), the solution was diluted by 80 ml of ethanol and kept for 10 h to deposit an AgNWs paste. This paste was put into a glass with 350 ml of distilled water for spinning with 6000 rpm for 30 min to get silver nanowires adhering to the glass walls. This AgNWs paste was removed from the glass and put into other glass with 200 ml of ethanol. By ultrasonic stirring, the AgNWs paste was dispersed completely in 2 h. Finally, 100 ml of distilled water was added into the AgNWs + ethanol solution; totally, 300 ml of the AgNWs solution was prepared for further studies.

Next, to prepare PEDOT-PSS + GQD + AgNW solutions, we used GQDs+PEDOT:PSS mixture with a volume ratio 2/1 of 10 wt.% GQDs solution/PEDOT:PSS, further this solution is called as GPA. Next step, to the GPA solution, a small amount of the AgNWs paste was added. The AgNWs pastes were dispersed in the GPA solutions by ultrasonic wave for at 65°C 1 h.

Using spin coating, GQC and GPA solutions were deposited onto glass substrates which were coated by two silver planar electrode arrays with a length (L) of 10 mm and separated each one from the other by a distance (l) of 5 mm, as shown in **Figure 1**. In the spin-coating technique used for preparing composite films, the following parameters were chosen: a delay time of 100 s, a rest time of 45 s, a spin speed of 1500–1800 rpm, an acceleration of 500 rpm, and finally, a drying time of 3 min. To dry the composite films, a flow of dried gaseous nitrogen was used for 10 h. For a solidification avoiding the use of solvents, the film samples were annealed at 120°C for 8 h in a "SPT-200" vacuum drier.

For simplicity in further analysis, the GPC sensor samples without and with CNT of 0.4, 0.8, and 1.2 wt.% were abbreviated to GPC-0, GPC-1, GPC-2, and GPC-3, respectively, whereas GPA sensors with AgNW of 0.2, 0.4, and 0.6 wt.% are called GPA1, GPA2, and GPA3, respectively.

http://dx.doi.org/10.5772/intechopen.79060

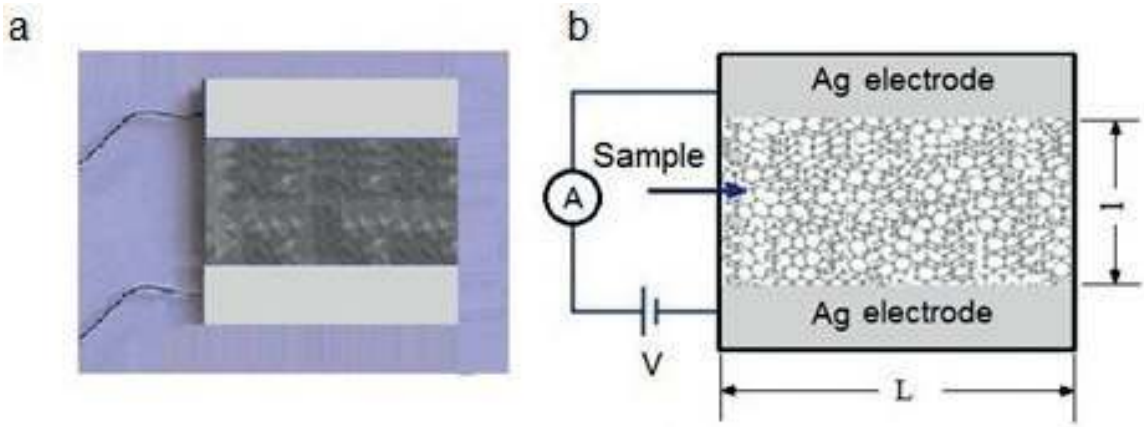

Figure 1. Image of a humidity sensor made from a single layer of composite films (a) and the schematic drawing of the device with the two planar electrodes (b). Humidity change is detected by the change in the current with a constant Dc-bias applied to the two electrodes.

2.1.2. Preparation of P3HT + rGO + CNT film sensors

All chemicals like PEDOT:PSS, P3HT, and multiple wall CNTs, with purity of ≥ 99.9% were purchased from Sigma-Aldrich Corporation. To prepare reduced graphene oxide (rGO), graphite flakes (GF) were taken off from graphite pieces with fewer layers by microwave heating solution of graphite filled in $KMnO_4$ and HNO_3. Mixtures of 0.2 g GF, 0.2 g $NaNO_3$, and 9.6 ml H_2SO_4 were put in a 200 mL volume Corning-247 glass beaker, then 1.2 g $KMnO_4$ and 28 ml of distilled water were poured into the glass beaker to get a liquid solution. Next, 10 ml H_2O_2 was added to this solution and ultrasonically stirred at room temperature for 8 h to separate MnO_4^- and MnO_2 into Mn^+ ions, yielding a solution with a bright-yellow color. The obtained solution was unmoved for 24 h, and at the glass beaker bottom, a paste-like layer with dark-yellow color was deposited, constituting the rGO paste. By slowly sucking, the solution above the rGO paste was completely taken from the glass beaker. Finally, 0.2 g of rGO paste was diluted in 40 ml of N,N-dimethylformamide (DMF) solvent in 50 ml-volume glass beaker and ultrasonically stirred for 900 s to get completely dispersive rGO in DMF (rGO-DMF). After 24 h waiting for the solution stabilization, 30 ml of rGO-DMF solution from the glass beaker top was taken and kept in another glass beaker for further use.

P3HT powder with a volume of 6 mg was mixed in 0.6 ml of rGO-DMF solution. This solution was ultrasonically stirred for 2 h at room temperature. At the same time, 1 mg of multiwalled carbon nanotubes (shortly called CNTs) was embedded in 0.5 ml of DMF (CNT-DMF) and also stirred by ultrasonic machine for 1 h. Finally, mixtures of the rGO-DMF and CNT-DMF solutions were put in a small glass beaker and carefully stirred for 5 h at 80°C by using a magnetic stirrer. For all the volumes of chemicals of P3HT, rGO, and CNTs used for further solid film preparation, the weight ratio of P3HT:rGO:CNTs was 100:20:10 (namely, the volume content of rGO and CNTs embedded in P3HT matrix was chosen to be, respectively, 20 and 10 wt.%. For simplicity in further analysis, the composite samples with such contents of P3HT, rGO, and CNTs were abbreviated to P3GC.

Using spin coating, P3GC solutions were deposited onto glass substrates which were coated by two silver planar electrode arrays with a length of 4 mm and separated from each other by a distance of 2 mm, which is similar to the image in **Figure 1**. The following parameters were used for spin coating: a delay time of 100 s, a rest time of 45 s, a spin speed of 1500–1800 rpm, an acceleration of 500 rpm, and finally a drying time of 300 s. To dry the composite films, a flow of dried gaseous nitrogen was used for 10 h. For a solidification avoiding the use of solvents, the film samples were annealed at 120°C for 2 h in a "SPT-200" vacuum drier. To compare the performance efficiency of P3HT + rGO + CNT with the one for PEDOT:PSS + rGO + CNT-based sensors, PEDOT:PSS + rGO + CNT composites (shortly called PEGC) were prepared by the abovementioned procedure with replacement of P3HT by PEDOT:PSS polymer.

2.2. Characterization techniques

The thickness of the films was measured on a "Veeco Dektak 6M" stylus profilometer. The size of GQDs and the surface morphology of the films were characterized by using "Hitachi" Transmission Electron Microscopy (TEM), Emission Scanning Electron Microscopy (FE-SEM), and NT-MDT atomic force microscope operating in a tunnel current mode. Crystalline structures were investigated by X-ray diffraction (XRD) with a Philips D-5005 diffractometer using filtered Cu-K_α radiation ($\lambda = 0.15406$ nm). The ultraviolet–visible absorption spectra were carried out on a Jasco UV–VIS–NIR V570.

For humidity sensing measurements, the samples were put in a 10 dm^3-volume chamber; a humidity value could be fixed in a range from 20 to 80% by the use of an "EPA-2TH" moisture profilometer (USA). The adsorption process is controlled by insertion of water vapor, while desorption process was done by extraction of the vapor followed by insertion of dry gaseous Ar. The measurement system that was described in [30] consisting of an Ar gas tank, gas/vapor hoses and solenoids system, two flow meters, a bubbler with vapor solution, and an airtight test chamber connected with collect-store data DAQ component. The Ar gas played a role as carrier gas, dilution gas, and purge gas.

For each sample, the number of measuring cycles was chosen to be at least 10 cycles. The humidity flow taken for measurements was of ~60 sccm ml/min. The sheet resistance of the samples were measured on a "KEITHLEY 2602" system source meter. To characterize humidity sensitivity of the composite samples, the devices were placed in a test chamber and device electrodes were connected to electrical feedthroughs.

For monitoring gases, the prepared sensing samples were put in a testing chamber of 10 dm^3 in volume. The gases value can be fixed in a rage from 10 to 1000 ppm by use of an "EPA-2TH" profilometer (USA). To characterize the gas sensitivity of the samples, the devices were placed in a test chamber at the room temperature (namely 300 K) and the Ar gas pressure of 101.325 kPa (or 1 Atm); the device electrodes were connected to electrical feedthroughs. The measurements that were carried out included two processes: adsorption and desorption. In the adsorption process, the gas (or vapor) flow consisting of Ar carrier and measuring vapor from a bubbler was introduced into the test chamber for an interval of time, following which the change in resistance of the sensors was recorded. In the desorption process, a dried Ar gas flow was inserted in the chamber in order to recover the initial resistance of the sensors. Through the recovering time dependence of the resistance, one can obtain information on the desorption ability of the sensor in the desorption process.

http://dx.doi.org/10.5772/intechopen.79060

The P3GC film sensors were exposed to NH_3 gas with concentration (C_{gas}) that was controlled with step decreases from 50 to 40, 30, 20, and 10 ppm. The repeatability in the resistance change of P3GC sensor was studied by measuring the resistance of sensor as a function of both the insertion/extraction of ammonia gas in/out chamber and measurement time. Each measurement cycle consists of the following time durations: 20 s for NH_3 gas detecting to saturation state, 50 s for maintaining exposed ammonia gas in chamber with abovementioned concentrations (namely C_{gas} = 50, 40, 30, 20, and 10 ppm), 30 s for extraction of Ar and ammonia gas out from chamber; then, 20 s for heating samples at 70°C for completing extraction of NH_3 and finishing the prior cycle. The next cycle was repeated by the same steps.

3. Results and discussion

3.1. PEDOT-PSS + GQD + CNT and PEDOT-PSS + GQD + AgNW

3.1.1. Electrical property and morphology of PEDOT-PSS + GQD + CNT and PEDOT-PSS + GQD + AgNW composite films

From a TEM micrograph of a GQDs sample (**Figure 2a**), it is seen that the size distribution of the dots is considerably homogenous, as evaluated in this micrograph, the dots size ranged from 10 to 15 nm. **Figure 2b** is an FE-SEM micrograph of the GPC-3 sample where the CNT and GQDs clearly appeared while the conjugate polymer PEDOT:PSS exhibited a transparent matrix. This SEM micrograph also shows that in the GPC composite film, there are mainly heterojunctions of the GQD/PEDOT-PSS and CNT/PEDOT:PSS, whereas CNT/GQD junctions are rarely formed.

From the thickness measurements, it can be seen that embedding CNT made the GPC samples considerably thicker. However, for the CNT-embedded GPC films, the CNT concentration was not much affected by the film thickness, so that the change in the thickness versus CNT

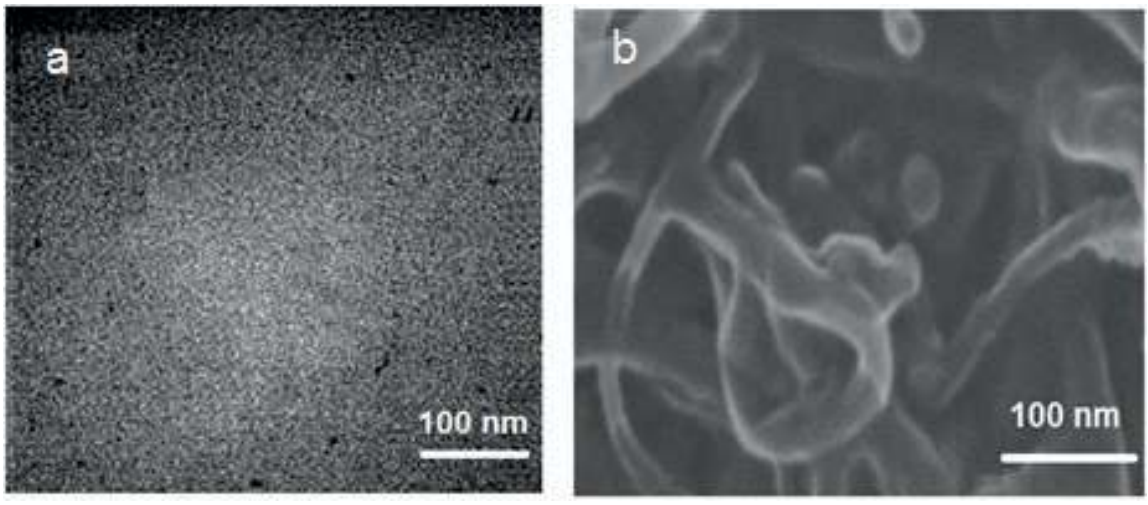

Figure 2. A TEM micrograph of GQDs sample (a) and FE-SEM of GPC-3 composite film (b) [29].

Samples	CNT content (wt.%)	Thickness, d (nm)	R_s (kΩ)	Conductivity, σ (S/cm)
GPC-0	0	460	2.180	4.98
GPC-1	0.4	485	2.160	4.76
GPC-2	0.8	487	0.814	7.93
GPC-3	1.2	490	0.356	27.52

Table 1. Thickness and resistance at room temperature of graphene quantum dots/CNT composite films [29].

concentration could be neglected. Indeed, for GPC-0 samples (i.e., the samples without CNT) the value of the film thickness was found to be ~5% smaller than that of the GPC + CNT samples (**Table 1**). This can be explained by the lower viscosity of GPC solution in comparison with the viscosity of GPC composite solutions. The results of measurements of the sheet resistance (R) of the samples are listed in **Table 1**.

The conductivity of the GPC-3 film is the largest and can be compatible to the conductivity of a pure PEDOT-PSS film as reported in [31]. Embedding GQDs and CNT into PEDOT-PSS has made the conductivity of PEDOT-PSS to decrease, leading to the expectation that the sensitivity of the GPC composite films would be enhanced. The temperature dependence of the conductivity of GPC samples is shown in **Figure 3**. For GPC-1 sample, σ versus T curves exhibit a typical property of the inorganic semiconductors: with increase in temperature, the conductivity increases. With increases in the CNT content, the composite exhibited a clearer semiconductor behavior; and when it reached a value as large as 1.2 wt.% (namely in GPC-3 sample), the conductivity of the films maintained an almost unchanged value of 37.2 S/cm

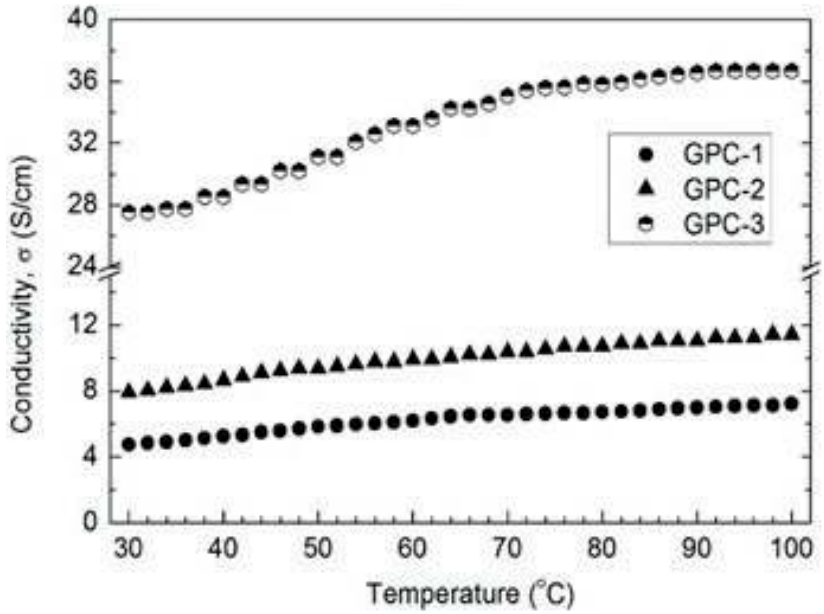

Figure 3. Temperature dependence of the conductivity of GPC-1, GPC-2 and GPC-3 films [29].

Samples abbreviation	AgNW content (wt.%)	Film thickness, d (nm)	Resistance at 50°C (MΩ)	Conductivity (S/m)
GPA1	0.2	450	4.56	0.024
GPA2	0.4	460	4.24	0.026
GPA3	0.6	480	3.88	0.027

Table 2. The data of the AgNWs-doped GQDs+PEDOT:PSS composite films used for humidity sensors [28].

under elevated operating temperatures. This thermal stability property is a desired factor for materials that are used in sensing applications.

The data of the samples including the AgNWs content, thickness, initial resistance, and conductivity are listed in **Table 2**. The value of the conductivity of the pure PEDOT:PSS film is ~80 S/cm as reported in [17] that is much larger than the one of the GPA composite films. This proves that the composite films possess a poor concentration of charge carriers. However, for materials used in gas sensing monitoring, this fact is an advantage in detecting a small amount of charge carries generated from adsorbed molecules, for instance, H_2O vapor.

FE-SEM image of AgNWs solution (**Figure 4a**) shows clearly the shape and dimension of the stick-like Ag wires, as evaluated in this image, the wire size is of 70 nm. **Figure 4b** is an FE-SEM image of the GPA3 film where the AgNWs and GQDs clearly appeared while the conjugate polymer PEDOT:PSS exhibited a transparent matrix. This SEM micrograph also shows that in the composite film, there are mainly heterojunctions of the GQD/PEDOT-PSS and AgNW/PEDOT:PSS, whereas AgNW/GQD junctions are rarely formed.

From our experiments, the temperature dependences of the resistance of AgNWs-doped GQDs+PEDOT:PSS composite films were found to be similar to those reported for CNTs-doped GQDs+PEDOT:PSS films [14]. With the increase of temperature, the AgNWs-doped composite exhibited the behavior of a heavily doped semiconductor: the resistance decreased

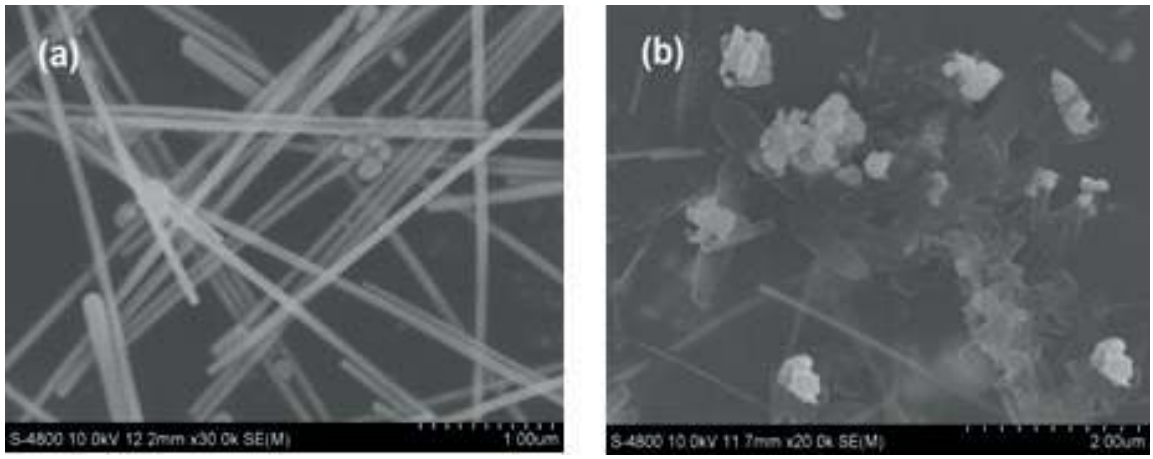

Figure 4. FE-SEM micrograph of an AgNWs containing solution (a) and surface of GPA3 film [28].

one order in magnitude from the initial values. Indeed, with the AgNWs content of 0.6 wt.% (GPA3), the resistance of the sensor lowered from 3.88 to 400 kΩ with increase of temperature from room temperature to 80°C and maintained a unchanged value of 350 kΩ under elevated (100–140°C) operating temperatures. This thermal stability is a desired factor for materials used in sensing applications.

3.1.2. Humidity sensing

3.1.2.1. For GPC

Figure 5 demonstrates the adsorption and desorption processes of the GQDs-PEDOT:PSS and CNT-PEDOT:PSS sensors. **Figure 5** shows that in the first 60 s, Ar gaseous flow eliminated the contamination agents from the GQDs-PEDOT:PSS surface, consequently the surface resistance increased. After the cleaning of the sensor surface during 30 s, the introduced humidity vapor was adsorbed onto the sensor surface, resulting in the decrease of the resistance. In the subsequent cycles, the humidity desorption/adsorption process led respectively to increase and decrease of the resistance of sensors, with results similar to those reported in [11]. However, through each cycle, the resistance of the GQDs-PEDOT:PSS film did not recover/restore to its initial value, but increased in 1–2 kΩ, to a final value of 235 kΩ after 1000 s from 220 kΩ. The increase in the initial resistance of the GQDs-PEDOT:PSS mainly related to the decrease of the major charge carriers in PEDOT:PSS. This is due to the elimination of holes (as the major carriers in PEDOT:PSS) by electrons that were generated from the H_2O adsorption. The

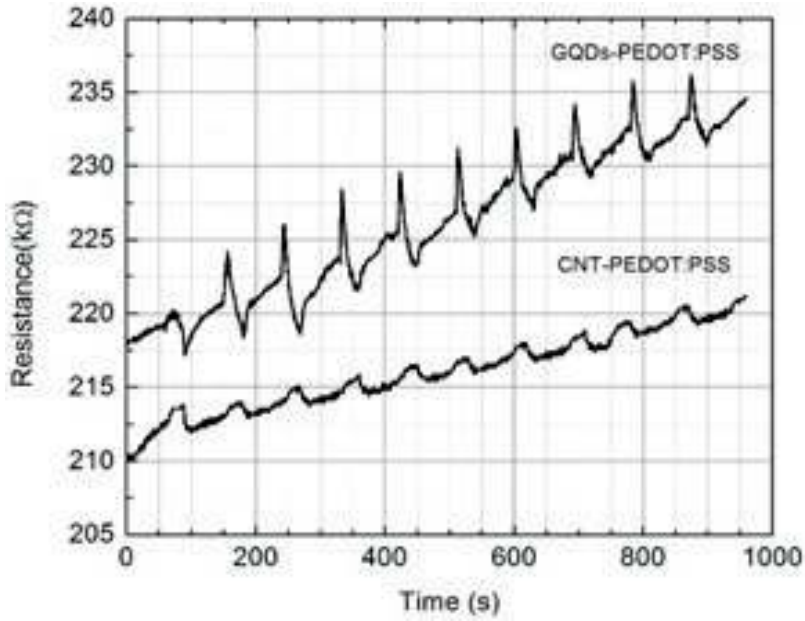

Figure 5. Sheet resistance change vs. humidity of GQDs-PEDOT:PSS and CNT-PEDOT:PSS composite films during adsorption/desorption processes [29].

more desorption/adsorption cycles, the more holes were eliminated in the deeper distances in the composite films. The similar feature in the sheet resistance change versus humidity was observed for the CNT-PEDOT:PSS, but the sensitivity of the last was much less than the one of the GQDs-PEDOT:PSS sensor. This proves the advantage of GQDs embedded in PEDOT:PSS polymer for the humidity sensing.

To evaluate sensing performance, a sensitivity (η) of the devices was introduced. It is determined by following equation:

$$\eta = \frac{R - R_o}{R_0}(\%) \tag{1}$$

The absolute magnitude of the sensitivity of the GPC-0 calculated by formula (3) is of ca. 2.5%.

Plots of time dependence of the sensitivity of the CNT-doped GPC composite films are shown in **Figure 6**. From **Figure 6**, one can see that for the GPC samples, vice versa to the GQDs-PEDOT:PSS, the humidity (i.e., H_2O vapor) adsorption process led to increase in the resistance of the films. Moreover, the resistance increased at a much faster rate than when it decreased.

Looking at the humidity sensing curves in **Figure 6**, one can distinguish two phenomena: the "rapid" (steep slope) and "slow" (shallow slope) response. The rapid response arises from H_2O molecular adsorption onto low-energy binding sites, such as sp^2-bonded carbon, and the slow response arises from molecular interactions with higher energy binding sites, such as vacancies, structural defects, and other functional groups [32, 33]. For the next step, the sensitivity ability of GPC composite was studied and the whole experiment process as described above was repeated. The data in **Figure 6** show that the presence of CNT can improve the sensing properties of GPC sheets. With increase in the CNT content, the resistivity increased, from 4.5% (for GPC-1) to 9.0% (for GPC-2) and 11.0% (for GPC-3).

The response time (i.e., the duration for R_o raising up to R_{max} in the adsorption process) for all three GPC sheets is almost the same value of 20 s, whereas the recovery time (the

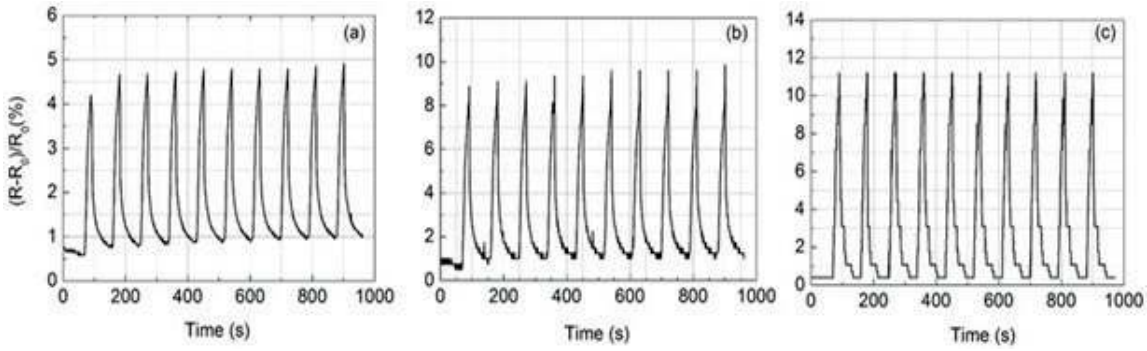

Figure 6. Comparison of the humidity sensing of the GPC composite-based sensors vs. CNT content; (a) GPC-1 (0.4 wt%), (b) GPC-2 (0.8 wt %) and (c) GPC-3 (1.2 wt.%) [29].

duration for R_o lowering to R_{max} in the desorption process) decreased from 70 s (GPC-1, **Figure 6a**) to 60 s (GPC-2, **Figure 6b**) and 40 s (GPC-3, **Figure 6c**). In addition, the complete H_2O molecular desorption on the surface of GPC composites took place at room temperature and atmospheric pressure. One can guess that connecting together, individual GPC sheets by CNTs caused the increase of the mobility of carriers in GPC composite films, consequently leading to higher H_2O vapor sensing ability of the CNT-doped GQDs-PEDOT:PSS composites. Indeed, due to the appearance of CNTs bridges, the number of the sites with high binding energies in GPC sheets decreases, while the number of those with low binding energies increases. Since the H_2O molecules was mainly adsorbed at the sites with low binding energies, the appearance of CNTs bridges led to the complete desorption ability of GPC composites.

3.1.2.2. For GPA

From experimental measurements, we have found that the electrical characteristics of our thin-film sensor elements are strongly dependent on the surrounding atmosphere, on humidity in particular. The increase in relative humidity results in significant decrease of the electrical resistance of the GPA composite films, namely GPA1, GPA2, and GPA3 (see **Figure 7**). At the RH lower 30%, the resistance of the sensors intensively decreased and reached an almost the same value of 400 kΩ from RH larger 50%. This demonstrates that AgNWs-doped GQDs+PEDOT:PSS composite films can be used well for humidity sensing in a range from RH10% to RH40%. Moreover, in this RH range, GRA3 sensor is the most sensitive to humidity, comparing to GRA1 and GRA2.

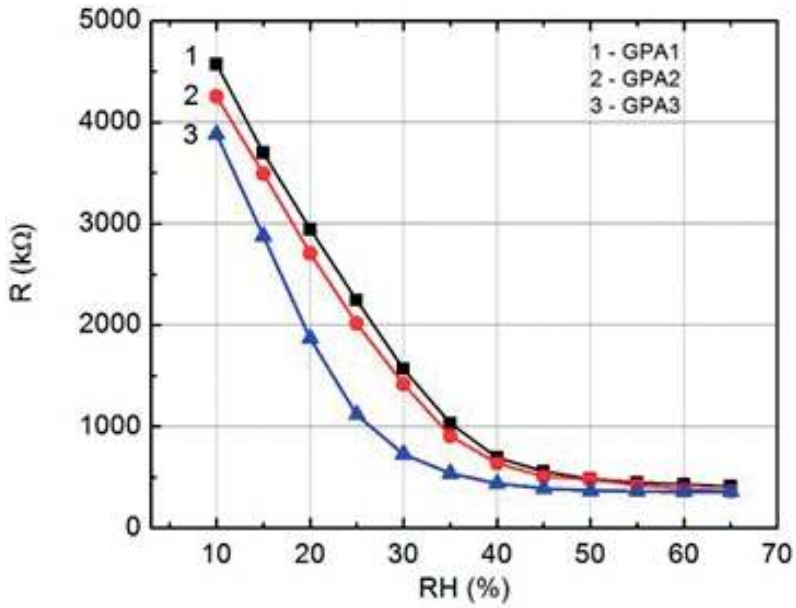

Figure 7. RH% dependence of the surface resistance of AgNWs-doped GQDs+PEDOT:PSS for three composite films with 0.2 wt.% (curve "1"), 0.4 wt.% (curve "2") and 0.6 wt.% of AgNWs (curve "3") [28].

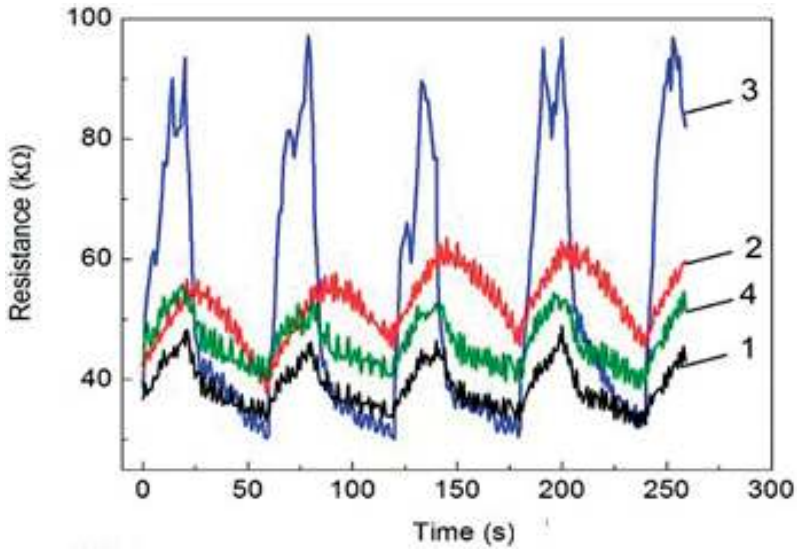

Figure 8. Responses of resistance of the sensors based on AgNWs-doped GQD/PEDOT:PSS films to the pulse of relative humidity (RH 30%) at room temperature for samples GPA1 (curve "1"), GPA2 (curve "2"), GPA3 (curve "3") and GPA1 (curve "4") [28].

The humidity dependence of the resistance of the hybrid (or composite) films can be explained by the interaction of water molecules with the surface of the composite, which leads to changing electric parameters of the GQDs. On the other hand, water impurities might induce additional or so called "secondary" doping of the conjugated polymer PEDOT:PSS. This manifests itself in change of the chain shape to an "unfolded spiral" and, therefore, stimulates increase in the conductivity [8].

More detailed measurements of the time response of the sensors were carried out in the conditions of H_2O vapor insertion and extraction, respectively, to the adsorption and desorption processes. **Figure 8** demonstrates the results of the measurements for AgNWs-doped GQDs+PEDOT:PSS sensors, i.e., for GPA1, GPA2, and GPA3. From **Figure 4**, one can see that the best humidity sensitivity was obtained in the sensor made from GPA3 film where the AgNWs content is of 0.6 wt.%. The samples with larger AgNWs contents (namely 0.8–1.2 wt.%) in the composites were also made; however, the sensing to humidity of these composite decreased rapidly. Indeed, in **Figure 8**, the adsorption and desorption processes of the 0.8 wt.% AgNWs-doped GQDs+PEDOT:PSS sensor (called as GPA4) were revealed worse than that of the GPA3 sensor (0.6 wt.% AgNWs). **Figure 8** shows that the humidity desorption/adsorption process led, respectively, to increase/decrease of the resistance of sensors, with results similar to those reported in [18].

Figure 9 shows the sensitivity determined by Formula (1) for the GPA3 sensor during 5 cycles of the adsorption and desorption of H_2O vapor. The absolute magnitude of the sensitivity of the GPA3 calculated by formula (3) reached a value as large as 15.2%. The plots for GPA1 and GPA2 sensors have a shape similar to the one of GPA3 (here they are not presented); however, the sensitivity was smaller, namely 5.5 and 6.5%, respectively, for

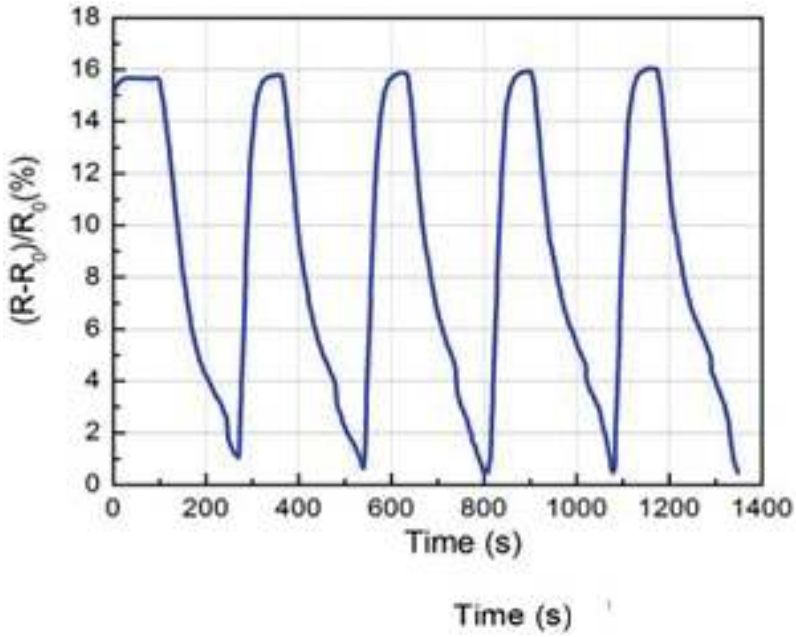

Figure 9. Responses of the sensitivity of the GPA3 sensor to the pulse of relative air humidity (RH30%) at room temperature [28].

GPA1 and GPA2. Comparing with the CNT-doped GQDs+PEDOT:PSS film sensor (η ~11%) as reported in [14], the humidity sensing of 0.6 wt.% AgNWs-doped composite is much larger.

In addition, the complete H_2O molecular desorption on the surface of GPA composites took place at room temperature and atmospheric pressure. One can guess that connecting together individual GPA sheets by AgNWs caused the increase of the mobility of carriers in composite films, consequently leading to higher H_2O vapor sensing ability of the AgNWs-doped GQDs+PEDOT:PSS composites. Similar to CNT-doped GQDs+PEDOT:PSS composites, due to the appearance of AgNWs bridges, the number of the sites with high binding energies in GPA sheets decreases, while the number of those with low binding energies increases. Since the H_2O molecules were mainly adsorbed at the sites with low binding energies, the appearance of AgNWs bridges led to the complete desorption ability of GPA composites.

3.2. NH_3 gas sensing

3.2.1. Film morphology and structures

Figure 10 shows AFM images of a pure P3HT and annealed P3GC composite films. The thickness of the film is 550 nm, the annealing temperature is 120°C and the annealing time is 2 h. **Figure 10a** shows that the pure P3HT film exhibited a smooth surface, whereas the roughness of the P3GC film surface was estimated as about 1.50 nm (**Figure 10b**). Thus, the roughness of the P3GC film can be attributed to the presence of both rGO and CNTs nanoparticles. The roughness and porosity of the composite sample were also observed by FE-SEM micrograph

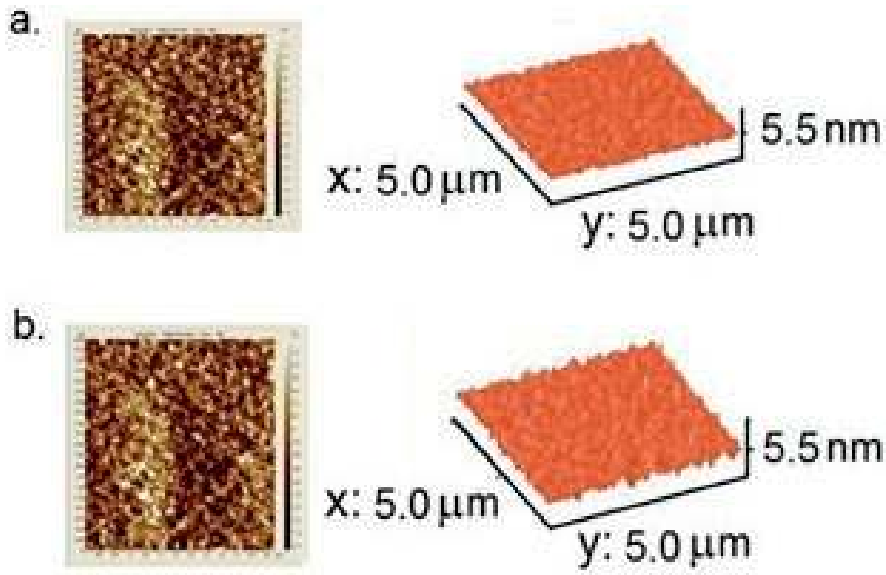

Figure 10. AFMs of a pure P3HT (a) and P3GC (b) film annealed at 120°C for 2 h.

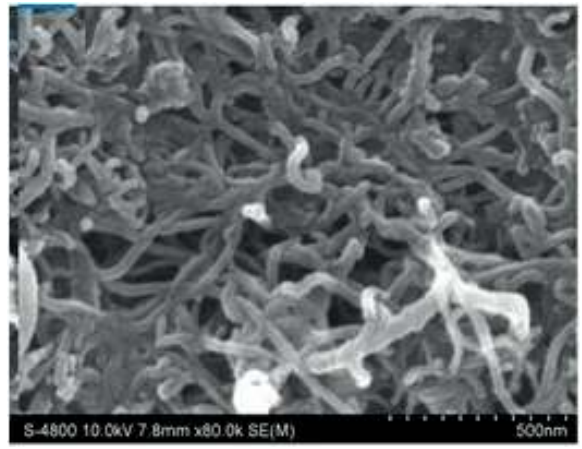

Figure 11. FE-SEM of a P3GC composite film.

(**Figure 11**) where P3HT polymer matrix is not revealed in the FE-SEM. **Figure 11** clearly shows the presence of the multiwalled carbon nanotubes in the P3GC sample.

3.2.2. Ammonia gas sensing

The results for the measurements of 5 cycles according to the ammonia concentration from 50, 40, 30, 20, and 10 ppm are shown in **Figure 12**. The cyclic behavior of the sensor performance shows that the P3GC sensors exhibited a good reversible sensing property toward ammonia gas. With exposition of ammonia gas in chamber, the sensor resistance increased rapidly, reaching the saturation value in about 20 s; and recovering its initial value in about 30 s after

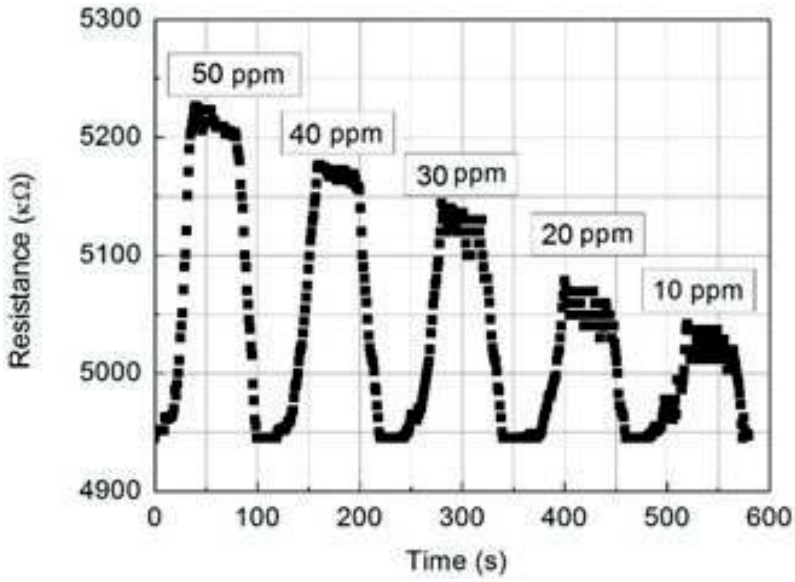

Figure 12. Time dependence of resistance of P3GC film on repeated exposure and removal of NH_3 gas.

the extraction of ammonia gas from the chamber. The increase in resistance of the P3GC sensor is closely related to a lowering of major charge carriers (namely holes) in P3HT polymer that is considered as a p-type organic semiconductor [34]. Whereas NH_3 is a highly active and electron-donating free radical [24], electrons generated by the absorption of ammonia gas on the surface of P3GC film eliminated a part of holes by coupling with each other, resulting in an increase of the P3HT resistance. When the P3GC film was slightly heated, NH_3 molecules in P3HT rapidly evaporated from the film surface, leaving holes along the backbone of the polymer. In such fashion, the concentration of major charge carriers rapidly increases while the resistance of the sensor decreases.

Embedding rGO in P3HT has enabled to enhance sensing properties of the P3GC films. This is similar to the results reported in [35] for polypyrrole (Py)-rGO-based sensors. Wang et al. explained the excellent sensing properties of Py-rGO-based sensors due to the parts of oxygen-based moieties and structure defects after chemical reduction process, resulting to the p-type semiconducting behavior of the resultant rGO. NH_3, as a reducing agent, has a lone electron pair that can be easily donated to the p-type rGO sheets, leading to the increase of the resistance of the rGO devices, whereas multiwalled CNTs have contributed to improve the adsorption efficiency of gas molecules (included NH_3) due to larger effective surface areas with many sites, as suggested by Varghese et al. [36]. Moreover, the addition of rGO and CNTs together in P3GC composite films created not only numerous nanoheterojunctions of P3HT/rGO and P3HT/CNT, but also nanotube "bridges" for electron transferring. These "bridges" are clearly revealed by the SEM micrograph, as shown in **Figure 11**.

In [4], we also demonstrated that inorganic nanoparticles embedded in polymers filled up most of the cracked spots in polymers that were often created during postannealing. By this way, the cracked spots served as charge traps were eliminated in nanocomposite films. With

the presence of nanoheterojunctions of P3HT/rGO and P3HT/CNT that together reduced the charge traps, one can enhance the performance of the sensors made from P3GC films.

From the sensitivity (η) of the P3GC sensor determined by Formula (1), the $\eta - C_{gas}$ dependence was plotted in **Figure 13**. The responding time of the sensor was about 30 s and the resistance of the P3GC composite films fast recovered to baseline when exposed to air. In the same period of time (namely 30 s), the sensing response to NH_3 with C_{gas} lowering from 50 to 40, 30, 20, and 10 ppm decreased from 2.9 to 2.4, 1.8, 1.3, and 0.8%, respectively.

Figures 12 and **13** show that the detection limit for NH_3 gas can attain a value is lower than 10 ppm. However, using the EPA-2TH gas profilometer, we could not introduce NH_3 gas with an accurate concentration in the range from 0 to 10 ppm. From **Figure 13**, one can see that the response of the sensor linearly decreases with decreases in ammonia gas concentration; and the slope of the linear plot reflects the relative sensitivity of the sensor. Thus, for the P3GC composite film sensor, the relative sensitivity was found to be of 0.05%/ppm. This value is still rather low, but it is about two times larger than the sensitivity of the ammonia gas sensor made from PEDOT: PSS [37].

Concerning the capacity for detecting ammonia gas in an environment that often has a relatively large humidity, we found that the P3HT-based sensor does not respond to humidity, whereas the PEDOT: PSS-based sensor is highly sensitive to this factor [29]. Indeed, this was confirmed by our results of the investigation on humidity (RH%) sensing of the two types of sensors, as a function of both the measurement time (**Figure 14**) and the relative humidity in the range from RH%20 to RH%65 (**Figure 15**).

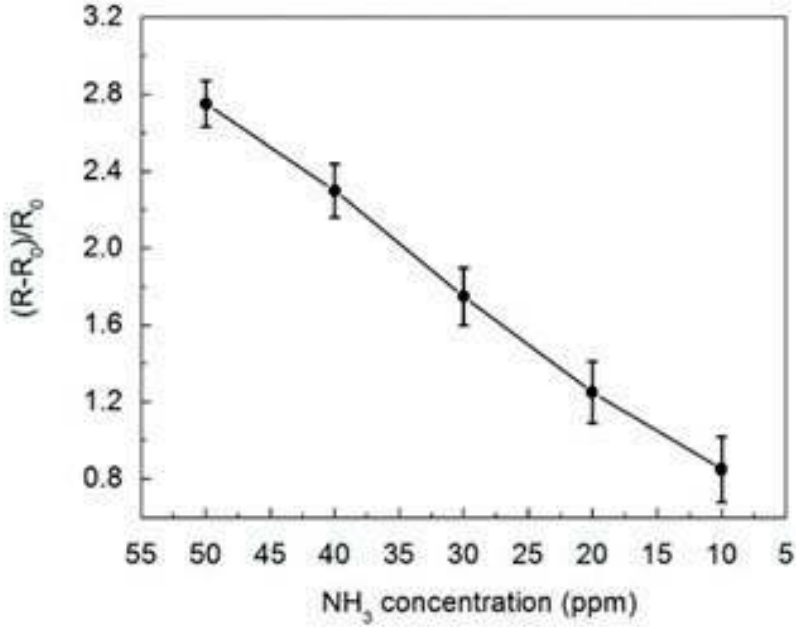

Figure 13. Sensitivity of P3GC sensor vs. ammonia concentration.

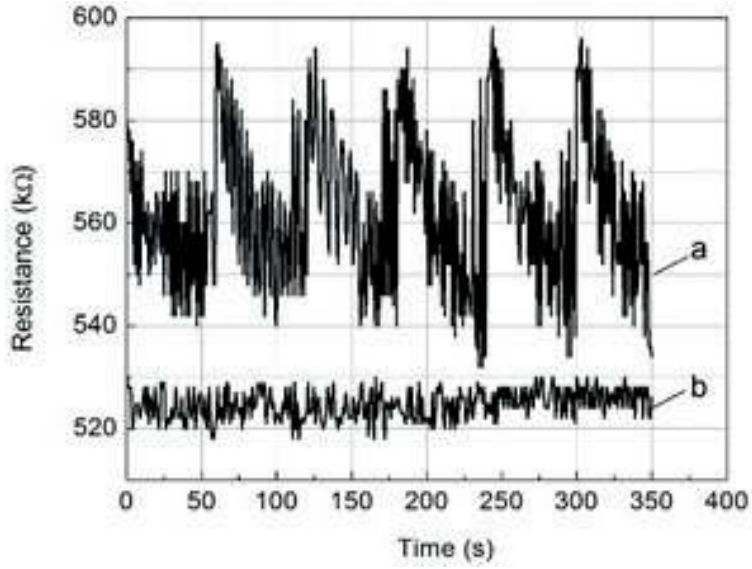

Figure 14. Comparison of the RH% sensitivity of PEGC (a) and P3GC sensors (b).

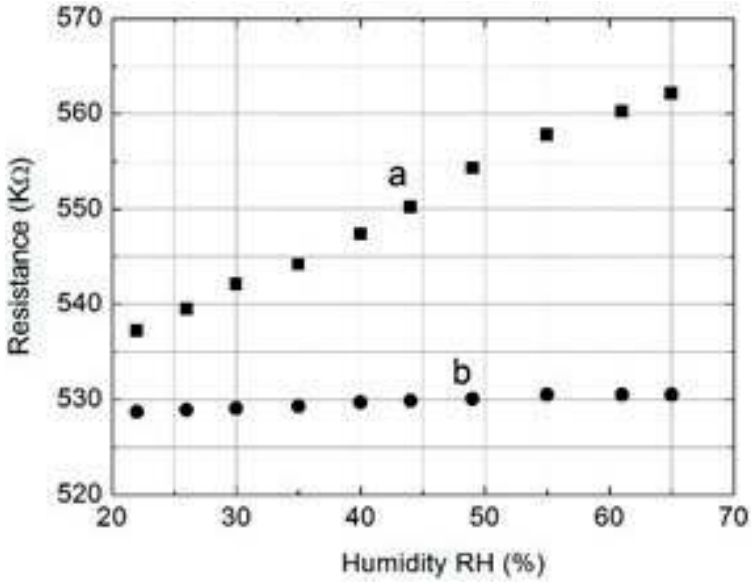

Figure 15. Humidity dependence of resistance of the PEGC (a) and P3GC films (b).

Although the ammonia gas response of P3GC sensors at 50 ppm (η = 2.9%) is lower compared to PEDOT: PSS-based sensors (η = 4.0% [28]), when one needs to monitor ammonia gas in a humid environment, P3HT/rGO/CNT (namely P3GC) sensors would be preferred. This is because signals obtained from measurements on PEDOT: PSS-based sensors would be undistinguishable between ammonia gas and water vapor.

4. Conclusion

- Using spin-coating technique, PEDOT: PSS + GQD + CNT (GPC), PEDOT: PSS + GQD + AgNW (GPA) films used for humidity sensors and P3HT + rGO + CNT (P3GC) films used for NH_3 gas sensors were prepared at room temperature and atmospheric pressure, all the sensing devices have extremely simple structure and they respond well to the humidity change (for GPC and GPA) and NH_3 gas (for P3GC).
- With the CNT content increase, from 0% (GPC-0) to 0.4 wt.% (GPC-1), 0.8 wt.% (GPC-2), and 1.2 wt.% (GPC-3), the sensitivity of the humidity sensing devices based on CNT-doped graphene quantum dot-PEDOT: PSS composites improved from 2.5% (GPC-0) to 4.5% (GPC-1), 9.0% (GPC-1), and 11.0% (GPC-2), respectively The response time of the GPC sensors was as fast as 20 s; and the recovery time of the sensors lowered from 70 s (0.4 wt.% CNT) to 60 s (0.8 wt.% CNT) and 40 s (1.2 wt.% CNT). With the AgNWs content increase, from 0.2 wt.% (GPA1) to 0.4 wt.% (GPA2) and 0.6 wt.% (GPA3), the sensitivity of the humidity sensing devices based on AgNWs-doped graphene quantum dot-PEDOT: PSS composites improved from 5.5% (GPA1), 6.5% (GPA2) and 15.2% (GPA3), respectively The best response time (~30 s) was obtained for sensors made from 0.6 wt.% AgNWs-doped GQDs+PEDOT: PSS composite films.
- P3GC (namely P3HT embedded with a content of 20 wt.% of rGO and 10% of CNTs) film sensors possessed a responding time of ca. 30 s, a sensing response of 0.8% at ammonia gas concentration of 10 ppm and a relative sensitivity of 0.05%/ppm. Investigation of humidity sensing of both the PEDOT: PSS + rGO + CNT and P3HT + rGO + CNT film sensors has demonstrated that P3HT + rGO + CNT film does not respond to humidity as it is the case for PEDOT: PSS + rGO + CNT. Useful applications in gas thin-film sensors for selectively sensing ammonia gas in a humid environment can thus be envisaged.

Acknowledgements

This research was funded by the Vietnam National Foundation for Science and Technology (NAFOSTED). The authors express sincere thanks to Prof. Dr. Vo-Van Truong (Concordia University, Canada) for useful discussions.

Author details

Nguyen Nang Dinh

Address all correspondence to: dinhnn@vnu.edu.vn

University of Engineering and Technology, Vietnam National University Hanoi, Hanoi, Vietnam

References

[1] Thomas PS, Kuruvilla J, Sabu T. Mechanical properties of titanium dioxide-filled polystyrene microcomposites. Materials Letters. 2004;**58**:281-289

[2] Móczó J, Pukánszky B. Polymer micro and nanocomposites: Structure, interactions, properties. Journal of Industrial and Engineering Chemistry. 2008;**14**:535-563

[3] Choulis SA, Mathai MK, Choong V-E. Influence of metallic nanoparticles on the performance of organic electrophosphorescence devices. Applied Physics Letters. 2006;**88**: 213503-213505

[4] Thao TT, Trung TQ, Truong V-V, Dinh NN. Enhancement of power efficiency and stability of P3HT-based organic solar cells under elevated operating-temperatures by using a nanocomposite photoactive layer. Journal of Nanomaterials. 2015;**2015**:7. Article ID 463565

[5] Huynh WU, Dittmer JJ, Alivisatos AP. Hybrid nanorod, polymer solar cells. Science. 2002;**295**:2425-2427

[6] Petrella A, Tamborra M, Cozzoli PD, Curri ML, Striccoli M, Cosma P, et al. TiO_2 nanocrystals – MEH-PPV composite thin films as photoactive material. Thin Solid Films. 2004;**451/452**:64-68

[7] Burlakov VM, Kawata K, Assender HE, Briggs GAD, Ruseckas A, Samuel IDW. Discrete hopping model of exciton transport in disordered media. Physical Review B. 2005; **72**:075206-1-075206-5

[8] Quyang J, Xu Q, Chu C-W, Yang Y, Li G, Shinar J. On the mechanism of conductivity enhancement in poly(3,4, ethylenedioxythiophene): Poly(styrene sufonate) film through solvent treament. Polymer. 2004;**45**:8443-8450

[9] Tehrani P, Kanciurzewska A, Crispin X, Robinson ND, Fahlman M, Berggren M. The effect of pH on the electrochemical over, oxidation in PEDOT:PSS films. Solid State Ionics. 2007;**177**:3521-3529

[10] Ummartyotin S, Juntaro J, Wu C, Sain M, Manuspiya H. Deposition of PEDOT: PSS nanoparticles as a conductive microlayer anode in OLEDs device by desktop inkjet printer. Journal of Nanomaterials. 2011;**2011**:7; Article ID 606714

[11] Gavgani JN, Dehsari HS, Hasani A, Mahyari M, Shalamzari EK, Salehi A, Taromi FA. A room temperature volatile organic compound sensor with enhanced performance, fast response and recovery based on N-doped graphene quantum dots and poly(3,4-ethylenedioxythiophene)–poly(styrenesulfonate) nanocomposite. Royal Society Of Chemistry. 2015;**5**:57559-57567

[12] Olenych IB, Aksimentyeva OI, Monastyrskii LS, Horbenko YY, Yarytska LI. Sensory properties of hybrid composites based on poly(3,4-ethylenedioxythiophene)-porous silicon-carbon nanotubes. Nanoscale Research Letters. 2015;**10**:187 (6p)

[13] Shen JH, Zhu YH, Yang XL, Li CZ. Graphene quantum dots: Emergent nanolights for bioimaging, sensors, catalysis and photovoltaic devices. Chemical Communications. 2012;**48**:3686-3699

[14] Zhang ZP, Zhang J, Chen N, Qu LT. Graphene quantum dots: An emerging material for energy-related applications and beyond. Energy & Environmental Science. 2012;**5**(10):8869-8890

[15] Li L, Wu G, Yang G, Peng J, Zhao J, Zhu J-J. Focusing on luminescent graphene quantum dots: Current status and future perspectives. Nanoscale. 2013;**5**:4015-4039

[16] Basu S, Bhattacharyya P. Recent developments on graphene and graphene oxide based solid state gas sensors. Sensors and Actuators B. 2012;**173**:1-21

[17] Yin PT, Kim TH, Choi JW, Lee KB. Prospects for graphene-nanoparticle-based hybrid sensors. Physical Chemistry Chemical Physics. 2013;**15**:12785-12799

[18] Chu BH, Nicolosi J, Lo CF, Strupinski W, Pearton SJ, Ren F. Effect of coated platinum thickness on hydrogen detection sensitivity of graphene-based sensors. Electrochemical and Solid-State Letters. 2011;**14**:K43-K44

[19] Zhang M, Wang Z. Nanostructured silver nanowires-graphene hybrids for enhanced electrochemical detection of hydrogen peroxide. Applied Physics Letters. 2013;**102**: 213104-213106

[20] Sreeprasad TS, Rodriguez AA, Colston J, Graham A, Shishkin E, Pallem V, Berry V. Electron-tunneling modulation in percolating network of graphene quantum dots: Fabrication, phenomenological understanding, and humidity/pressure sensing applications. Nano Letters. 2013;**13**:1757-1763

[21] Hibbard T, Crowley K, Killard AJ. Direct measurement of ammonia in simulated human breath using an inkjet-printed polyaniline nanoparticle sensor. Analytica Chimica Acta. 2013;**779**:6-63

[22] Gardon M, Guilemany JM. A review on fabrication, sensing mechanisms and performance of metal oxide gas sensors. Journal of Materials Science. 2013;**24**:1410-1421

[23] Janata J, Josowicz M. Conducting polymers in electronic chemical sensors. Nature Materials. 2003;**2**(1):19-24

[24] Bai H, Shi G. Gas sensors based on conducting polymers. Sensors. 2007;**7**(3):267-307

[25] Patois T, Sanchez J-B, Bergeretal F. Elaboration of ammonia gas sensors based on electrodeposited polypyrrole-cobalt phthalocyanine hybrid films. Talanta. 2013;**17**:45-54

[26] Lee Y-S, Joo B-S, Choi N-J, Lim J-O, Huh J-S, Lee D-D. Visible optical sensing of ammonia based on polyaniline film. Sensors and Actuators B. 2003;**93**(1-3):148-152

[27] Basu S, Bhattacharyya P. Recent development on graphene and graphene oxide based solid state gas sensors. Sensors and Actuators B. 2012;**173**:1-21

[28] Long LM, Dinh NN, Thu HT, Phong HT, Trung TQ. Characterization of humidity sensing of polymeric graphene-quantum-dots composites incorporated with silver nanowires. VNU Journal of Science: Mathematics-Physics. 2017;**33**(3):52-60

[29] Long LM, Dinh NN, Trung TQ. Synthesis and characterization of polymeric graphene-quantum-dots based nanocomposites for humidity sensing. Journal of Nanomaterials. 2016;**2016**(2016):6; Article ID 5849018

[30] Trung TQ, Huynh TMH, Tong DT, Van Tam T, Dinh NN. Synthesis and application of graphene–silver nanowires composite for ammonia gas sensing. Advances in Natural Sciences: Nanoscience and Nanotechnology. 2013;**4**:045012-1-045012-4

[31] Quyang J, Chu C-W, Chen F-C, Xu Q, Yang Y. High-conductivity poly(3,4-ethylenedioxythiophene): Poly(styrene sulfonate) film and its application in polymer optoelectronic devices. Advanced Functional Materials. 2005;**15**:203-208

[32] Lu G, Park S, Yu K, Ruoff RS, Ocola LE, Rosenmann D, Chen J. Toward practical gas sensing using highly reduced graphene oxide: A new signal processing method to circumvent run-to-run and device-to-device variations. ACS Nano. 2011;**5**:1154-1164

[33] Robinson JT, Perkins FK, Snow ES, Wei Z, Sheehan PE. Reduced graphene oxide molecular sensors. Nano Letters. 2008;**8**:3137-3140

[34] Omer BM. Optical properties of poly (3-hexylthiophene-2,5-diyl) and poly (3-hexylthiophene-2,5-diyl)/[6,6]-phenyl C61-butyric acid 3-ethylthiophene ester thin films. Journal of Nano and Electronic Physics. 2013;**5**(3):03010-1-03010-4

[35] Wang Y, Zhang L, Hu N, Wang Y, Zhang Y, Zhou Z, Liu Y, Shen S, Peng C. Ammonia gas sensors based on chemically reduced graphene oxide sheets self-assembled on au electrodes. Nanoscale Research Letters. 2014;**9**:12; Article 251

[36] Varghese OK, Kichambre PD, Gong D, Ong KG, Dickey EC, Grimes CA. Gas sensing characteristics of multi-wall carbon nanotubes. Sensors and Actuators B. 2001;**81**(1):32-41

[37] Aba L, Yusuf Y, Mitrayana, Triyana K. Selectivity improvement of gas sensor based on poly(3,4-ethylenedioxythiophene): Poly(styrenesulfonate) thin film by using imprinting method. Journal of Modern Physics. 2012;**3**:529-533